Supplementary Information

A bottom-up route to enhance thermoelectric figures of merit in graphene nanoribbons

Hâldun Sevinçli, Cem Sevik, Tahir Çağın, Gianaurelio Cuniberti

Supplementary Information on Methods

1.1 DFTB Calculations of Electrons and Phonons

In this work, electronic Hamiltonians and overlap matrices as well as the interatomic force constants are obtained using the density functional tight binding (DFTB) method as implemented in the DFTB+ sofware package[1]. The advantage of the DFTB approach, when compared to genuine density functional methods, is its accuracy and efficiency in the calculation of systems with large unit cells. As shown in Figure 1a, the calculated phonon dispersions of 2D graphene by using finite displacement scheme[2] and the experimental results (see Ref. 3) shows the accuracy of DFTB in describing the vibrational properties of sp2 carbon structures. The electronic bands are also well decribed with DFTB (see Figure 1).

In Figure 2, we show the electronic bands, DOS (a, c) and ballistic electron transmission spectra (b, d) for s-GNR (a, b) and c-GNR (c, d). Likewise, phonon dispersions and transmission spectra of s-GNR and c-GNR are plotted in Figure 3. In Figure 3a and 3c phonon dispersions and ballistic transmissions are shown except dispersionless high frequency C-H modes lying above 3000 cm^{-1}. Figures 3b and 3d are close-ups to lower energy modes that dominate vibrational heat transport. The fundamental effect of chevron geometry is the formation of mini-bands in electron and phonon dispersions, which results in a subsequent increase of van Hove singularities in the densities of states and narrowing of ballistic transmission plateaus. As a result the electronic structure of c-GNR becomes more compatible with Mahan-Sofo criteria and phonon transmission is substantially reduced due to the fragmented dispersions and geometry induced energy gaps.

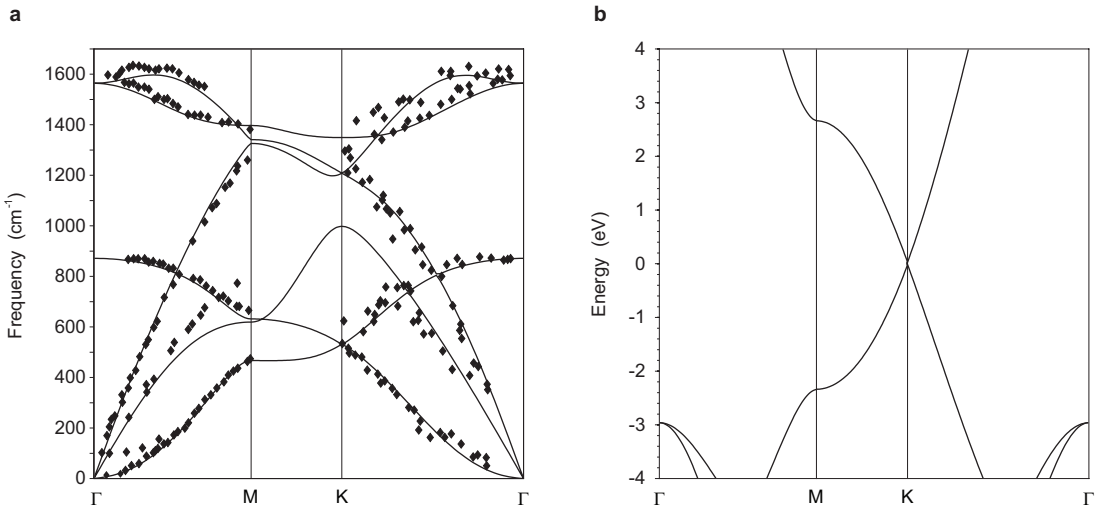

Figure 1: Phonon dispersions (left) and electronic bands (right) of graphene as calculated by using the DFTB approach. Diamonds in (a) represent the experimental data.

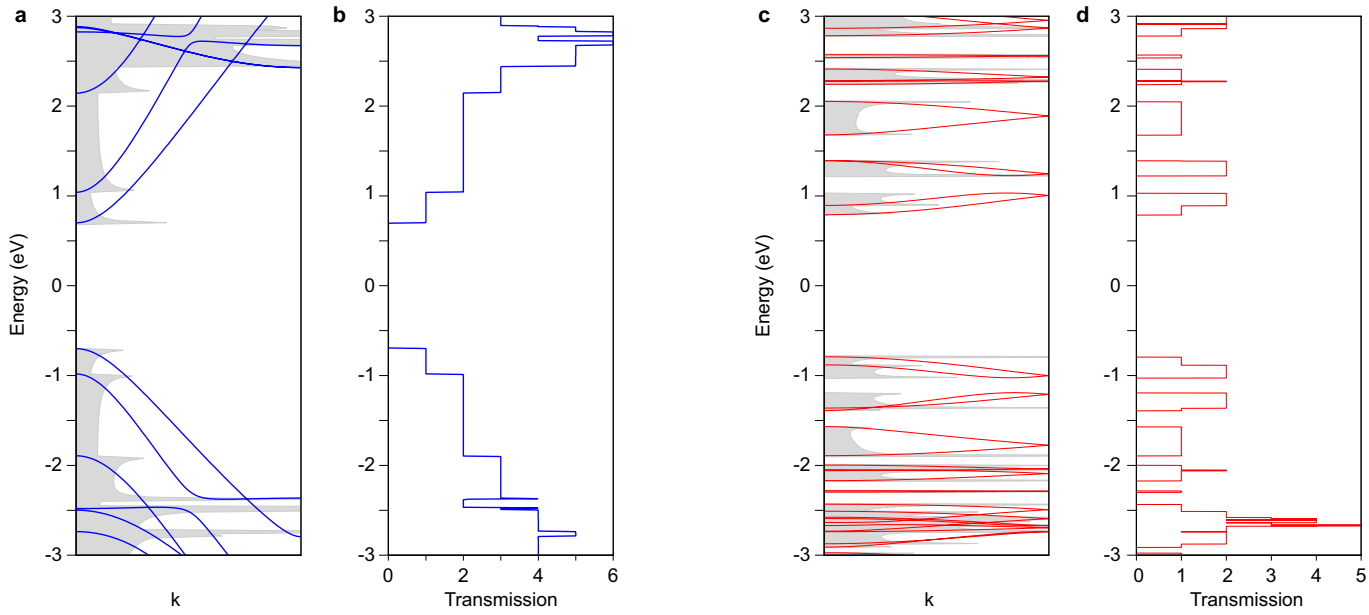

Figure 2: Electronic bands, densities of states and ballistic transmission spectra of s-GNR (a,b) and c-GNR (c,d).

1.2 Nonequilibrium Green's Functions (NEGF)

The partitioning scheme is employed in transport calculations, where the system is divided into three regions as the central disordered region (C) and the left and right pristine reservoirs (L and R) of the same material. Having obtained the Hamiltonian H and the overlap matrix S from DFTB simulations, the retarded GF is defined as

$$G^r_{\rm el}(E) = [\varepsilon S - H]^{-1}, \tag{1}$$

where $\varepsilon = E + i\delta$ and δ being an infinitesimal real positive number. Using the identity

$$\begin{pmatrix} \varepsilon S_{LL} - H_{LL} & \varepsilon S_{LC} - H_{LC} & 0 \\ \varepsilon S_{CL} - H_{CL} & \varepsilon S_{CC} - H_{CC} & \varepsilon S_{CR} - H_{CR} \\ 0 & \varepsilon S_{RC} - H_{RC} & \varepsilon S_{RR} - H_{RR} \end{pmatrix} \begin{pmatrix} G^r_{LL} & G^r_{LC} & G^r_{LR} \\ G^r_{CL} & G^r_{CC} & G^r_{CR} \\ G^r_{RL} & G^r_{RC} & G^r_{RR} \end{pmatrix} = 1, \tag{2}$$

the retarded GF of the central region is expressed as

$$G^r_{{\rm el},CC}(E) = (\varepsilon S_{CC} - H_{CC} - \Sigma^r_L - \Sigma^r_R)^{-1} \tag{3}$$

with

$$\Sigma^r_{{\rm el},L/R}(E) = (\varepsilon S_{CL/CR} - H_{CL/CR}) G^{r,0}_{{\rm el},LL/RR} (\varepsilon S_{LC/RC} - H_{LC/RC}) \tag{4}$$

being the self energies due to coupling to the reservoir states. Here, $G^{r,0}_{{\rm el},LL/RR} = (\varepsilon S_{LL/RR} - H_{LL/RR})^{-1}$ are the surface GF of the semi-infinite free reservoirs and they are calculated using the iterative scheme as explained in Ref. 4. Having obtained the broadening functions $\Gamma_{L/R} = i(\Sigma^r_{L/R} - \Sigma^a_{L/R})$, the lesser and greater self energies are defined as

$$\Sigma^<_{L/R} = f_{\rm FD}(E - \mu_{L/R}, T)\Gamma_{L/R}, \tag{5}$$

$$\Sigma^>_{L/R} = [1 - f_{\rm FD}(E - \mu_{L/R}, T)]\Gamma_{L/R}, \tag{6}$$

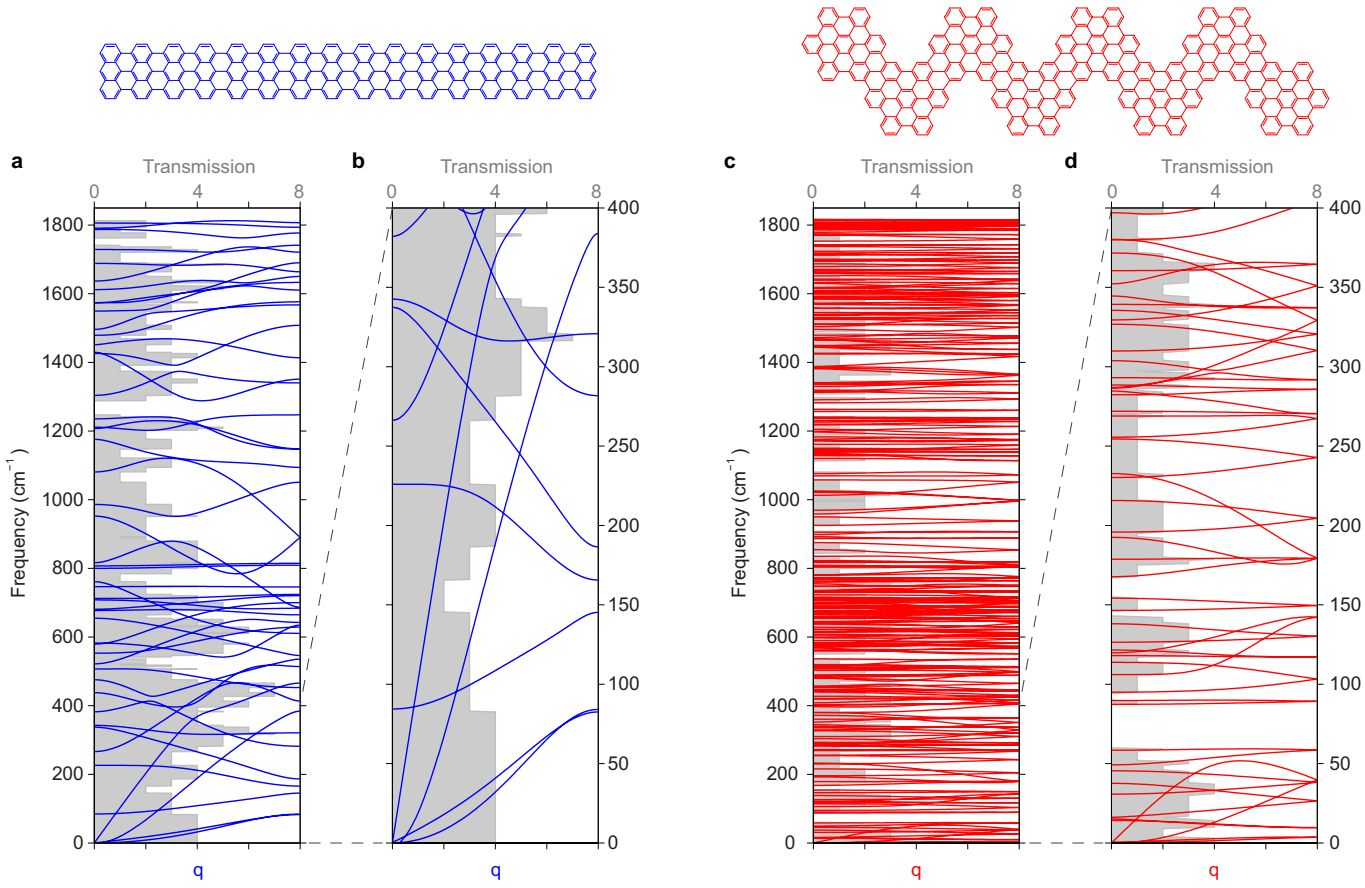

Figure 3: Phonon dispersions and ballistic phonon transmission spectra of s-GNR (a,b) and c-GNR (c,d), whose geometries are sketched on top. (b) and (d) are close-ups to lower energies that have the major contribution in thermal transport.

by using Fermi-Dirac distribution function f_{FD} and chemical potentials $\mu_{L/R}$. Correspondingly, the lesser and greater GFs are

$$G^{<}_{\mathrm{el}} = G^{r}_{\mathrm{el}}(\Sigma^{<}_{L} + \Sigma^{<}_{R})G^{a}_{\mathrm{el}}, \tag{7}$$

$$G^{>}_{\mathrm{el}} = G^{r}_{\mathrm{el}}(\Sigma^{>}_{L} + \Sigma^{>}_{R})G^{a}_{\mathrm{el}} \tag{8}$$

and the advanced GF G^{a}_{el} is obtained by setting $\varepsilon = E - i\delta$ in Equations 3 and 4. Electrical current is written as

$$I = -\frac{2e}{h}\int dE\, \mathrm{Tr}[\Sigma^{>}G^{<} - \Sigma^{<}G^{>}], \tag{9}$$

and the transmission spectrum in the coherent limit is obtained by setting $\mu_L = 1$ and $\mu_R = 0$ with

$$\mathcal{T}_{\mathrm{el}} = \mathrm{Tr}[\Sigma^{<}G^{>} - \Sigma^{>}G^{<}]. \tag{10}$$

The scatterings in the central region are taken into account through implementation of the recursion algorithm as explained in Section 1.4

1.3 Atomistic Green's Functions

Phonon transport properties are calculated using the AGF method, which is an efficient tool for addressing phonon scatterings at boundaries, interfaces and disordered systems, especially in reduced dimensions. The system is parti-

tioned as the central region and the reservoirs as is done for electrons, with the central part being isotopically disordered, and left and right reservoirs are semi-infinite pristine GNRs. Calculating the elements of the force constant matrix K in the harmonic approximation, AGF is defined in terms of the dynamical matrix $D = M^{-1/2}KM^{-1/2}$ as

$$G_{\rm ph}(\omega) = [(\omega^2 + i\delta)\mathbb{1} - D], \tag{11}$$

where M is the diagonal matrix of corresponding atomic masses and $\mathbb{1}$ is the identity matrix.

Similar to the case of electronic GFs, the GF of the central region is

$$G_{{\rm ph},CC}(\omega) = [(\omega^2 + i\delta)\mathbb{1} - D - \Sigma_L - \Sigma_R] \tag{12}$$

with $\Sigma_{L/R} = D_{CL/CR}G_{{\rm ph},LL/RR}D_{LC/RC}$ being the self energies due to reservoirs. Calculating the broadening of vibrational modes as

$$\Gamma_{L/R} = -2{\rm Im}\,\Sigma_{L/R} \tag{13}$$

the transmission spectrum is obtained from

$$\mathcal{T}_{\rm ph} = {\rm Tr}[\Gamma_L G_{{\rm ph},CC}\Gamma_R G^{+}_{{\rm ph},CC}]. \tag{14}$$

In both electronic and phononic calculations, the bottleneck is the computation of GF of the central region, which are carried out using the recursion scheme.

1.4 Recursion Scheme

Electron and phonon GFs of GNRs as long as 5 μm, consisting of more than 300,000 atoms, are not possible to compute with direct inversion of the matrices of the central region. The recursion scheme explained below is an efficient and numerically exact way of handling such large matrices. Here, we summarize the decimation of electronic GFs using nonorthogonal basis sets. Its implementation to phonons is straightforward. The Hamiltonian and the overlap matrix of the central region can be written in block tridiagonal form as

$$H = \begin{pmatrix} H_{11} & H_{12} & 0 & \dots & 0 & 0 \\ H_{21} & H_{22} & H_{23} & \dots & 0 & 0 \\ 0 & H_{32} & H_{33} & \dots & 0 & 0 \\ \vdots & \vdots & \vdots & \ddots & \vdots & \vdots \\ 0 & 0 & 0 & \dots & H_{N-1,N-1} & H_{N-1,N} \\ 0 & 0 & 0 & \dots & H_{N,N-1} & H_{N,N} \end{pmatrix} \tag{15}$$

$$S = \begin{pmatrix} S_{11} & S_{12} & 0 & \dots & 0 & 0 \\ S_{21} & S_{22} & S_{23} & \dots & 0 & 0 \\ 0 & S_{32} & S_{33} & \dots & 0 & 0 \\ \vdots & \vdots & \vdots & \ddots & \vdots & \vdots \\ 0 & 0 & 0 & \dots & S_{N-1,N-1} & S_{N-1,N} \\ 0 & 0 & 0 & \dots & S_{N,N-1} & S_{N,N} \end{pmatrix} \tag{16}$$

Similarly the retarded GF is written as

$$G = \begin{pmatrix} G_{11} & \dots & G_{1N} \\ \vdots & \ddots & \vdots \\ G_{N1} & \dots & G_{N,N} \end{pmatrix}. \tag{17}$$

Starting from the second cell, the effective Hamiltonians and the corresponding $G^{(n)}$ of the $(n+1)$st recursion step are

$$G^{(n)} = (\varepsilon S_{n+2,n+2} - H^{(n)}_{n+2,n+2})^{-1}, \quad (18)$$

$$H^{(n+1)}_{11} = H^{(n)}_{11} + (\varepsilon S_{n+1,n+2} - H^{(n)}_{1,n+2})G^{(n)}(\varepsilon S_{n+2,n+1} - H^{(n)}_{n+2,1}), \quad (19)$$

$$H^{(n+1)}_{1,n+2} = (\varepsilon S_{n+1,n+2} - H^{(n)}_{1,n+2})G^{(n)}(\varepsilon S_{n+1,n+2} - H^{(0)}_{n+1,n+2}), \quad (20)$$

$$H^{(n+1)}_{n+2,1} = (\varepsilon S_{n+2,n+1} - H^{(0)}_{n+2,n+1})G^{(n)}(\varepsilon S_{n+2,n+1} - H^{(n)}_{n+2,1}), \quad (21)$$

$$H^{(n+1)}_{n+2,n+2} = H^{(0)}_{n+2,n+2} + (\varepsilon S_{n+2,n+1} - H^{(0)}_{n+2,n+1})G^{(n)}(\varepsilon S_{n+1,n+2} - H^{(0)}_{n+1,n+2}), \quad (22)$$

with $n = 0, \ldots, N-3$. Repeating the decimation $N-2$ times, one arrives at the equivalent GF for the central region which consists of only G_{11}, G_{1N}, G_{N1}, and G_{NN}. For phonons, one sets $\varepsilon = (\omega^2 + i\delta)$, $S = \mathbb{1}$ and $H \to D$.

1.5 Thermoelectric Coefficients

Thermoelectric coefficients are defined in the linear response regime using the integral functions

$$L_n = \frac{2}{h}\int dE \left(-\frac{\partial f(E,\mu,T)}{\partial E}\right)(E-\mu)^n \mathcal{T}_{\rm el}(E). \quad (23)$$

with n being integers.[5] Electric conductance in the linear response regime can be expressed as $\mathcal{G}(\mu,T) = e^2 L_0$ while the Seebeck coefficient and the electronic contribution to heat conductance are

$$S(\mu,T) = \frac{1}{eT}\frac{L_1}{L_0} \quad (24)$$

$$\kappa_{\rm el}(\mu,T) = \frac{1}{T}\left(L_2 - \frac{L_1^2}{L_0}\right) \quad (25)$$

and the thermoelectric figure of merit is

$$ZT = \frac{\mathcal{G}S^2T}{\kappa_{\rm el} + \kappa_{\rm ph}}. \quad (26)$$

Supplementary Data

2.1 Phonon Mean-Free-Paths

In Figures 4 and 5 phonon mean free paths $\ell_{\rm ph}$ with different isotopes and densities are compared for s-GNR and c-GNR, respectively. We consider $d = 10\%$ and 50% of ^{14}C isotopes with atomic and precursor distributions. The details of $\ell_{\rm ph}(\omega)$ are mainly due to the phonon DOS of the structures. Highly oscillating behavior of $\ell_{\rm ph}$ for c-GNRs in the entire spectrum and vanishing $\ell_{\rm ph}$ values at certain energies are rooted in the increased number of singularities in DOS and the energy gaps. For both types of GNRs, precursor distributions yield longer $\ell_{\rm ph}$ at higher frequencies for a given isotope density and vice versa at lower frequencies (see the insets of Figure 5). Since it is mainly the low frequency modes which contribute thermal conduction, high frequency phonons having longer $\ell_{\rm ph}$ with precursor distribution do not affect the resulting $\kappa_{\rm ph}$, but reduced $\ell_{\rm ph}$ of low frequency phonons does. Comparison of low frequency $\ell_{\rm ph}$ of s-GNR and c-GNR at a given d shows that c-GNR has shorter $\ell_{\rm ph}$ by approximately one order of magnitude in the average.

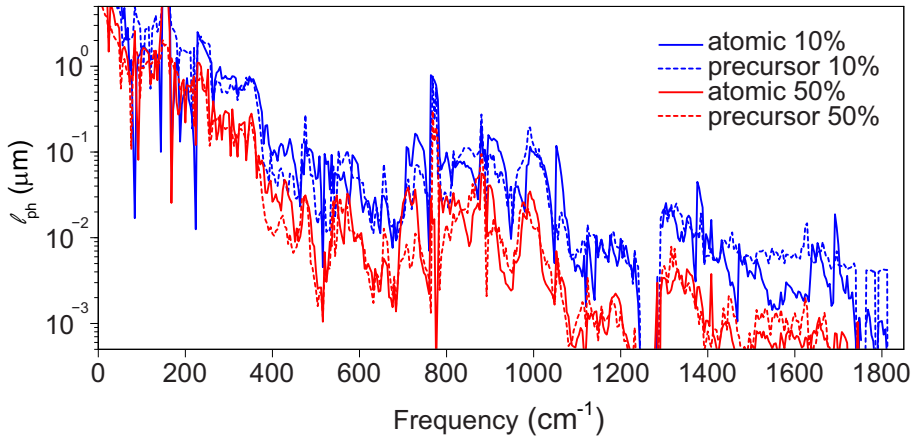

Figure 4: Phonon mean-free-paths for isotopically disordered s-GNR with different distributions and densities. The solid curves stand for atomic distributions, where the dotted lines are for precursor distributions.

2.2 Thermoelectric Coefficients

Investigation of the ballistic regime is a prerequisite for a detailed study of the effects of nano-structuring on thermoelectric transport. In this section we present thermoelectric properties of c-GNR within the ballistic assumption for both electrons and phonons; also considering the case when phonons are scattered by isotopic clusters while the electrons stay ballistic. Finally the details of TE coefficients are presented when scatterings are included for both electrons and phonons.

Ballistic Electrons and Phonons– The effect of geometry on TE transport in c-GNR is evident in the ballistic limit for both electrons and phonons. The power factor P is as high as 1 μW/K^2 and $\kappa_{\rm ph}/A$ is lower by more than a factor of 3 compared to s-GNR, yielding significantly high ZT values (Figure 6) (see also Ref. 6). Phonons being dominant in κ at μ where ZT is maximized, points to the possibility of significantly higher ZT upon phonon engineering, *i.e.* inclusion of heavy precursors.

Ballistic Electrons and Non-ballistic Phonons– The merit of isotope engineering is best visible when ballistic electron assumption is kept and phonons are scattered from heavy precursors with $d = 50\%$. Since G, S and P remain the same with those in Figure 6, only κ and ZT are shown in Figure 7. Vast reduction of κ at the charge neutrality point is purely due to the suppression of phonons. It is clear that, thermal transport is dominated by electrons for the whole range of μ where P is appreciably high (see also Figure 6c). As a result, ZT values higher than 3 are calculated for all $T = 300$ K, 500 K and 800 K for devices of lengths L =430 nm, 140 nm and 75 nm. We note that, these L correspond to the optimum system lengths when electron scatterings are included (cf. Figure 8). If all L are set to 5 μm and ballistic electron limit is considered, the ZT values can be as high as 4.9, 7.2 and 11 for $T = 300$ K, 500 K and 800 K, respectively.

Anderson Disorder– In Figure 8, electrical conductance $\mathcal{G}$, Seebeck coefficient S, power factor P, thermal conductance per cross section κ/A and ZT are plotted at T =300, 500 and 800 K for optimal c-GNR lengths that yield the highest ZT. Optimal L are due to the trade off between increasing thermal resistance and decreasing power factor with L. ZT is enhanced by a factor of 4 compared to the ballistic limit without isotope engineering and Anderson disorder, while it is reduced by 32% when compared to the ballistic electron limit.

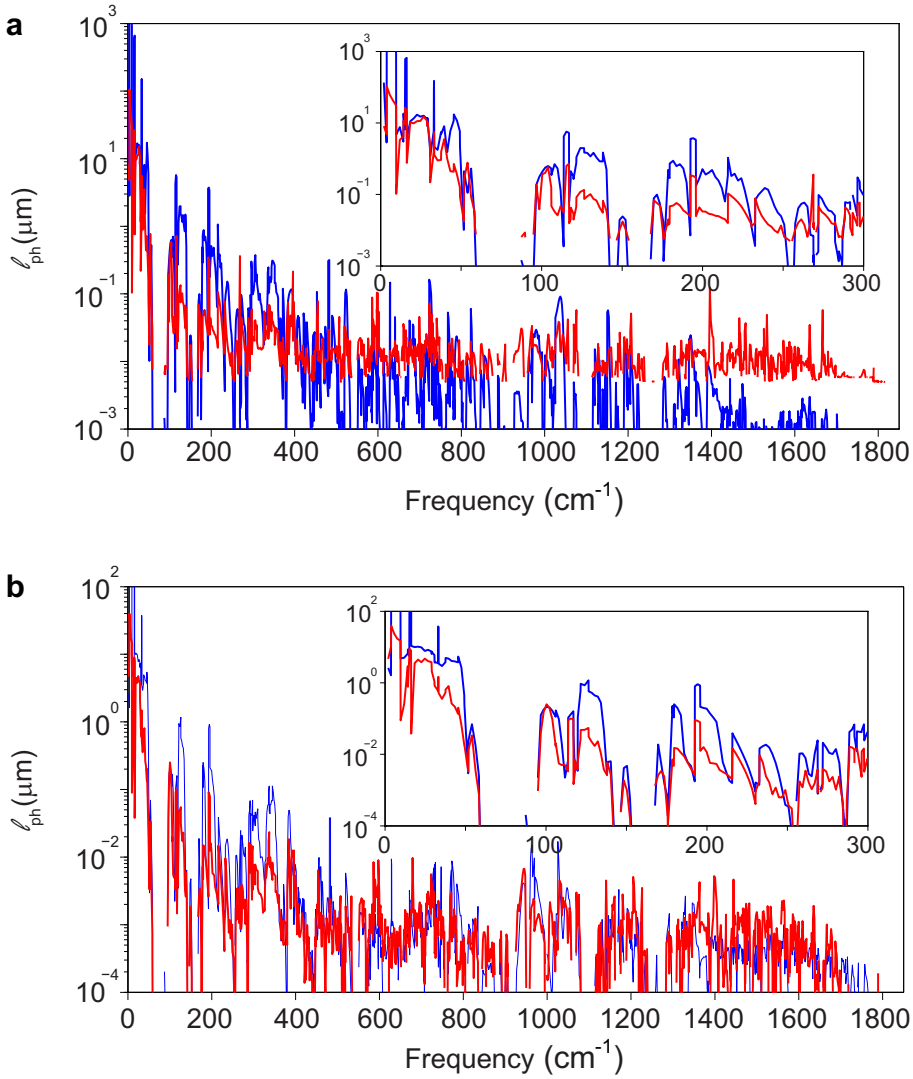

Figure 5: Phonon mean-free-paths of c-GNR for atomic (blue) and precursor (red) distributions of isotopes with densities $d = 10\%$ (a) and $d = 50\%$ (b). The insets show the lower energy mean-free-paths.

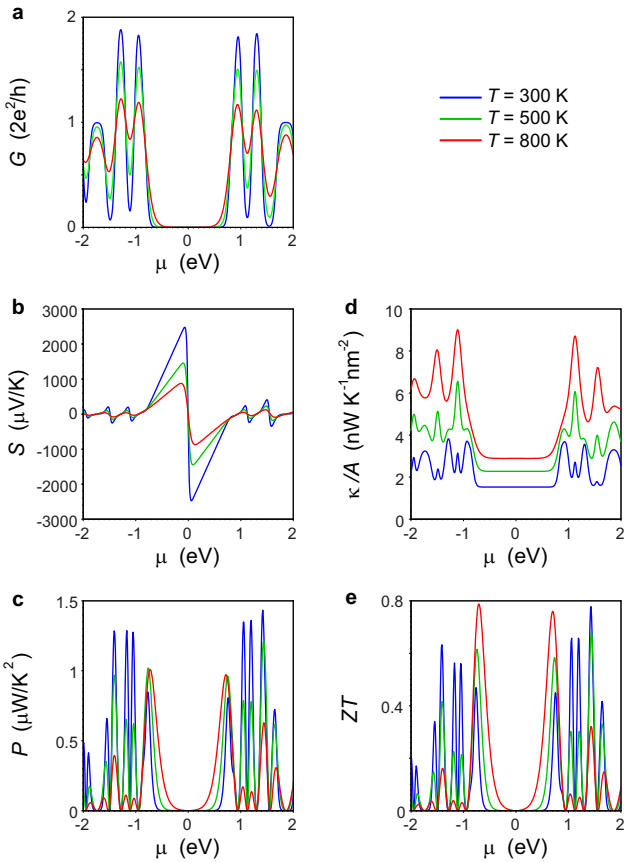

Figure 6: Electrical conductance (a), Seebeck coefficient (b), power factor (c), thermal conductance per cross section area (d), and TE figure of merit (e) for pristine c-GNR at different temperatures, T = 300 K (blue), 500 K (green), and 800 K (red).

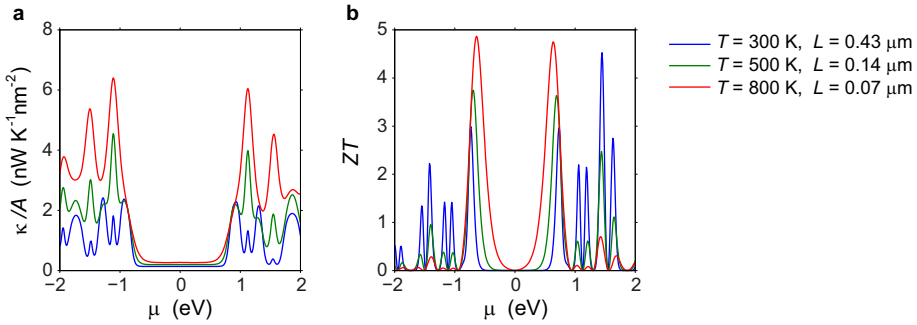

Figure 7: (a) Thermal conductance, κ/A, and (b) figure of merit, ZT, for c-GNR with heavy precursor distribution ($d = 50\%$) are plotted with assuming ballistic electron transmission at three different temperatures, T =300 K (blue), 500 K (green) and 800 K (red) with corresponding system lengths of L =0.43 μm, L =0.14 μm, and L =0.07 μm, respectively. See also Figures 6 and 8.

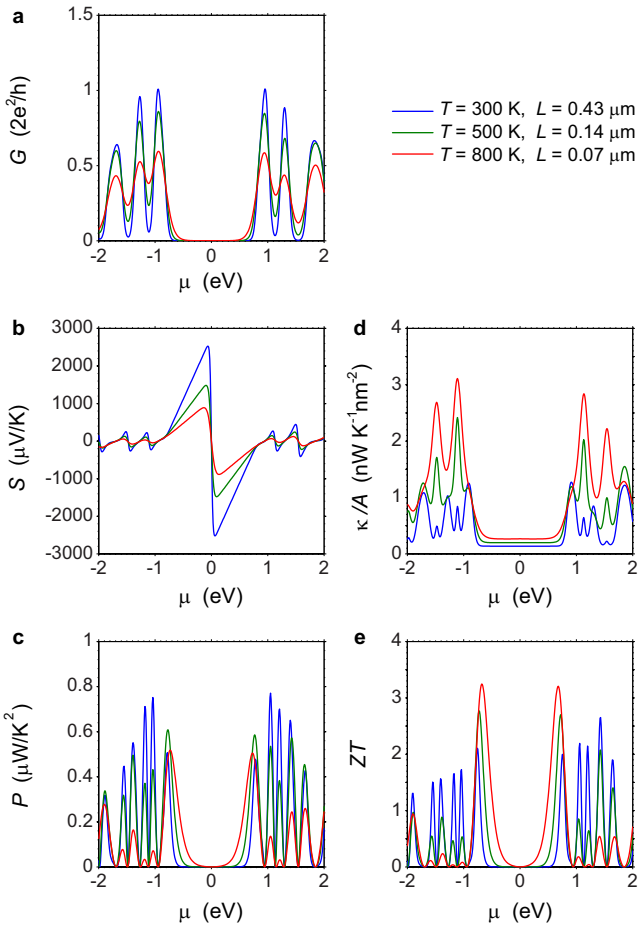

Figure 8: Electrical conductance (a), Seebeck coefficient (b), power factor (c), thermal conductance per cross section area (d), and TE figure of merit (e) for c-GNR with heavy precursors ($d = 50\%$) and Anderson disorder $w_A = \sqrt{12}k_{\rm B}T$ at $T = 300$ K (blue), 500 K (green) and 800 K (red) are plotted for optimum system lengths, L =0.43 μm, L =0.14 μm, and L =0.07 μm.

References

[1] Frauenheim, T. *et al.* A self-consistent charge density-functional based tight-binding method for predictive materials simulations in physics, chemistry and biology. *physica status solidi (b)* **217**, 41–62 (2000).

[2] Togo, A., Oba, F. & Tanaka, I. First-principles calculations of the ferroelastic transition between rutile-type and $cacl_2$-type sio_2 at high pressures. *Phys. Rev. B* **78**, 134106 (2008).

[3] Dubay, O. & Kresse, G. Accurate density functional calculations for the phonon dispersion relations of graphite layer and carbon nanotubes. *Phys. Rev. B* **67**, 035401 (2003).

[4] Sancho, M. P. L., Sancho, J. M. L., Sancho, J. M. L. & Rubio, J. Highly convergent schemes for the calculation of bulk and surface green functions. *Journal of Physics F: Metal Physics* **15**, 851 (1985).

[5] Esfarjani, K., Zebarjadi, M. & Kawazoe, Y. Thermoelectric properties of a nanocontact made of two-capped single-wall carbon nanotubes calculated within the tight-binding approximation. *Phys. Rev. B* **73**, 085406 (2006).

[6] Chen, Y., Jayasekera, T., Calzolari, A., Kim, K. W. & Nardelli, M. B. Thermoelectric properties of graphene nanoribbons, junctions and superlattices. *Journal of Physics: Condensed Matter* **22**, 372202 (2010).